FUDMA Journal of Engineering and Technology
ISSN: 3092-9385
https://sites.google.com/fudutsinma.edu.ng/fjet
Volume 1, Issue 2, 2025, 402-416

Gamma Shielding Capabilities of Some Selected Materials Within Ibadan Metropolis

Oluwadare J. AKINDUGBAGBE[1*], Adefope OWOJORI[2], Emmanuel AGBENYI[3], Babatunde ADEBO[4]

[1*,2,3,4]Department of Physics, Lead City University, Ibadan, Oyo State, Nigeria

[1*]jakindugbagbe@gmail.com, [2]owojori.adefope@lcu.edu.ng, [3]agbenyiodahemmanuel@gmail.com, [4]agbenyiodahemmanuel@gmail.com

Abstract

Conventional gamma shielding materials like lead are effective but present limitations related to cost, weight, and fabrication have prompted the need for locally accessed shielding materials. This study evaluates the gamma shielding potential of four locally-sourced materials; sawdust composite, acrylic, clay, and glass readily available within Ibadan metropolis. The elemental composition of each material was determined using ICP-OES and CHNO analyzers. Shielding parameters including linear attenuation coefficient (LAC), half-value layer (HVL), tenth-value layer (TVL), mean free path (MFP), and lead equivalence were estimated theoretically at 661 keV (Cs-137). Experimental HVL values were determined from the spectral response of NaI(Tl) gamma detector as gamma photons from a standard Cs-137 source was attenuated using the locally-sourced materials. From the result of the study, Glass had the highest estimated LAC (0.169 cm^{-1}), followed by clay (0.159 cm^{-1}), sawdust composite (0.153 cm^{-1}), and acrylic (0.095 cm^{-1}). Theoretical HVL values for glass, sawdust composite, clay and acrylic were estimated at 4.10 cm. 4.54 cm, 4.37 cm and 7.31 cm respectively. Experimental HVL values obtained for glass, sawdust composite, clay and acrylic differed from theoretical values by 3.73%, 0.87%, 2.99 % and 11.73%. Glass exhibited the lowest theoretical TVL (13.62 cm) and MFP (5.92 cm), indicating its superior shielding performance. In addition, a total thickness of about 55 cm would be needed to shield the gamma radiation from an active Cs-137 source completely and about 98 cm thickness of acrylic material to shield from the Cs-137 source completely. Due to its density, clay and sawdust may offer more practical alternatives for field use as they are optimally efficient in thicknesses. These findings suggest that locally sourced non-metallic materials can provide viable alternatives to conventional shielding materials in certain gamma radiation environments.

Keywords: *Gamma shielding, linear attenuation coefficient, Ibadan, glass, acrylic, clay, sawdust.*

1.0 Introduction

Radiation shielding is essential in an environment where artificial source of ionizing radiation is operational. Ionizing radiation is a type of radiation that has enough energy to break an electron away from an atom. They include X-rays, or gamma (γ-) rays. When ionizing radiation interacts with human cells, it could result to molecular changes in human cells thereby destructing the functions and structure of the cell. Hence, ionizing radiation is detrimental to humans and other living organisms. To reduce health risks within such facility, several measures and protocols have to be adhered to. The ALARA (As Low As Reasonably Achievable) principle, first articulated by the National Council on Radiation Protection and Measurements (NCRP) in 1954, advocates for minimizing human exposure to ionizing radiation by adhering to three core strategies: maximizing distance from radiation sources, minimizing the duration of exposure, and employing appropriate shielding measures. This framework is particularly critical in the context of gamma radiation, which, due to its high penetration capability, poses substantial health and environmental risks when not adequately contained. Gamma photon interacts differently with different material by photoelectric effect, Compton scattering or pair production depending on the photon energy. These events directly or indirectly lead to attenuation of the photons. To investigate the attenuation characteristics of a material, its elemental attenuation properties are considered. The search for shielding materials against harmful radiation in the nuclear and medical fields have been on for a long time (Chen, 2021). While Lead (Pb) seems to offer the most desirable gamma (γ-) shielding properties of known elements in nature, Studies also have shown that lead is largely not desirable in many applications due to their toxicity, high density, cost and difficulty in fabrication or deployment. Other promising alternative γ-shielding materials have also shown drawbacks, for instance, the bulk and low-density properties of concrete, the brittleness of ceramics, and the limited mechanical strength of bricks (Rilwan, 2024). Many have been localized to certain sections of the gamma facility based on the desired properties targeted to the material's functional properties of each section. Flat wood planks bonded with millimeters of Lead have been used as gamma shielding materials for certain rooms in medical facilities in numerous medical facilities in Ibadan metropolis (Okereke, 2024). Shielding Wood planks bonded with millimeters of Lead as well as other wood composites such as sawdust-based composites (wood-plastics composite) are not as effective as lead or other dense materials but offer more environmentally friendly and potentially cost-effective alternative for certain shielding applications.

Received: 02/08/2025; Revised: 10/08/2025; Accepted: 15/08/2025; Published: 15/09/2025

Wood sawdust, a by-product of the process of shaping timber and reducing its size, is one of these wastes. Each year millions of m^3 of wood sawdust, which contains lignin and cellulose, is produced. This waste is generally disposed of by burning or landfilling, both of which can cause serious environmental problems such as air pollution or land occupation. Various studies have been conducted on the evaluation of wood sawdust as a recycled material (Sevich, 2021). It is possible to reuse sawdust in the production of sawdust composites (Ninyong et al.,2019; Shamsuzzaman et al., 2019; Muhammad et al.,2022). Clay have been extensively studied (Olukotun et al., 2021; Hanfi et al., 2025) for their low weight and versatility. Their properties make them great base materials for radiation shielding[1]. When it comes to the need for γ- radiation shielding and optical transparency, glass and glass composites have been found suited for applications where transparent monitoring of gamma radiation is required (Zhao and Wang, 2013; Rawat et al., 2019). Glass materials contain high atomic number (Z) elements which help to provide superior radiation protection due to their influence on the density of the glass. Glass materials can be undesirable for use in certain areas of the γ-facility where optimal impact resistance, lightweight, and weather durability properties are top priorities. In such case, a polymer such as Polymethyl methacrylate (PMMA) also known as acrylic will be a desirable glass substitute. There have been studies on polymers (Ahmed et al.,2024; Toto et al., 2024; Abualrooset al.,2024) for gamma shielding more especially Acrylic and its composites Álvarez-Cortez et al. (2024). Consequently, research into alternative shielding materials that are cost-effective, light-weight, locally sourced, and environmentally friendly has become a necessary venture in both medical, nuclear and industrial applications. A number of naturally occurring or locally fabricated materials such as red clay, sawdust composites, glass and acrylic etc., have frequently been proposed in recent studies as potential alternatives to conventional shielding substances. These materials offer ease of access, local availability, and shielding capability of any material is typically quantified through parameters such as flexibility in shaping, casting or layering. The shielding capability of any material is typically quantified through parameters such as the linear attenuation coefficient (LAC), half-value layer (HVL), tenth-value layer (TVL), mean free path (MFP) and lead equivalence. These can be carried out experimentally using ratio of spectra at a certain known energy value or by using theoretical means (Tekin *et al.* 2022). These values determine the level of gamma photon penetration through the material and the penetration is incident photon energy-dependent (Bouzarjomehri *et al.*,2006), the density of the shielding material, and its elemental composition.

This study focuses on assessing and comparing the gamma shielding potentials of four selected materials commonly found within the Ibadan metropolis: glass, acrylic, red clay, and sawdust composite. The elemental compositions of these materials were analyzed using ICP-OES and C-H-N-O analyzers at the International Institute of Tropical Agriculture (IITA), Ibadan. The weight fractions of these elements are used with energy dependent mass attenuation coefficients (Al-khawlany *et al.*, 2019) derived from NIST database (Berger *et al.*, 2018), in calculating the linear attenuation coefficients. Theoretical HVLs, TVLs, MFPs were estimated. Experimental determinations and theoretical evaluations of shielding parameters were carried out using a Cs-137 gamma source (661 keV) at the Centre for Energy Research and Development (CERD), Obafemi Awolowo University Ile-Ife, and the values were compared with theoretical values.By analyzing the results of these materials in comparison to standard shielding benchmarks like lead, this study aims to propose viable, cost-effective shielding options for gamma protection in medical, industrial, and research applications within resource-limited gamma radiation facilities.

2.0 Methodology

Four locally available materials; sawdust composite, glass, red clay and acrylic were used for their potential use as alternative gamma radiation shields within Ibadan metropolis. The samples were prepared and processed as follows:

Sawdust Composite

Sawdust was collected from a local sawmill, ground into powder and mixed with Styrofoam glue. The mixture was cast into square shapes 2 cm x 2 cm at various thicknesses (1.35 cm to 7.55 cm). The samples were left to dry for three weeks before analyses.

Glass and Acrylic

Glass and acrylic sheets of different thickness 1 cm to 8cm and 0.15 cm to 10.25 cm, respectively, were sourced from local fabricators in Ibadan. These were cut into $4cm^2$ flat pieces for uniformity during irradiation.

Clay

Locally source clay was ground, mixed with water, molded into cylindrical shapes of 2 cm radius and left to dry. Sample thicknesses range from 1.25 cm to 6.15 cm

Received: 02/08/2025; Revised: 10/08/2025; Accepted: 15/08/2025; Published: 15/09/2025

Elemental analysis of each sample was conducted at International Institute of Tropical Agriculture (IITA) Ibadan. Two analytical methods were employed; the Inductively coupled plasma-optical emission spectrometry (ICP-OES) [Michalak *et al.*,2021] and CHNO Analyzer (Silva *et al.*, 2012)
For the experimental setup for attenuation measurement, Gamma shielding measurements were conducted at the Centre for Energy Research and Development (CERD), Obafemi Awolowo University, Ile-Ife. Cs-137 source (661keV) and a NaI(TI) scintillation detector were used. Each sample was irradiated for 30 minutes and the transmitted intensity was measured. Stacked samples were used to achieve varying thicknesses.

Theoretical Background

The gamma shielding properties were determined based on standard radiation transport equations and attenuation models. Using the mixture rule (Elmahroug *et al.*, 2013)

$$\left(\frac{\mu}{\rho}\right)=\sum_i w_i \left(\frac{\mu}{\rho}\right)_i \tag{1}$$

where $\frac{\mu}{\rho}$ is the mass attenuation coefficient of the compound/mixture, $\left(\frac{\mu}{\rho}\right)_i$ is the ith element's mass attenuation coefficient w_i is the weight fraction of the ith element in the compound or mixture and $\sum_i$ is a summation term over a number, i

Linear attenuation coefficient $\mu_c(E)$ of a composite or mixture/compound is probability per unit length for a photon (gamma) to interact with the material compound/mixture. It is calculated from the mass attenuation coefficient $\left(\frac{\mu}{\rho}\right)_{c(E)}$ (Waly et al., 2016; Jawad et al., 2019).,

$$\left(\frac{\mu}{\rho}\right)_{c(E)} \tag{2}$$

$$\mu_c(E) = \left(\frac{\mu}{\rho}\right)_{c(E)} . \rho \tag{3}$$

where $\rho\ is\ density\ in\ g/cm^3$ and w_i are individual elemental weight fractions

The energy-dependent theoretical Half-Value Layer, $HVL(E)_i$, for any compound mixture or element is defined in terms of a factor of thickness with which a photon beam had been reduced into half of its initial intensity. It is expressed in terms of the linear attenuation coefficient as:

$$HVL(E)_{i_{Th}} = \frac{0.693}{\mu_i(E)_{Th}} \tag{4}$$

The theoretical Tenth-Value Layer, $TVL(E)_i$, for any compound mixture or element, can then be calculated using (Niksarlıoğlu et al., 2023).

$$TVL(E)_{t_{Th}} = \frac{2.30259}{\mu_i(E)_{Th}} \tag{5}$$

Energy-dependent Mean free path (MFP) is used to assess shielding competence. It is expressed in equation (6) as (Axeez *et al.*, 2013, Niksarlıoğlu et al., 2023)

$$MFP(E) = \frac{1}{\mu(E)} \tag{6}$$

The energy-dependent experimental HVL $HVL(E)_{Expt}$, is given as $X_{0.5^{I}/_{I_o}}$, calculated from the thickness (in cm) at 50% relative-intensity value ($50\%\ ^{I}/_{I_0}$) in equation (7) and the interpolated HVL thickness is extracted from the Attenuation curve using Microsoft® excel interpolation function

$$HVL(E)_{Expt} = Thickness_{50\%^{I}/_{I_0}} = X_{0.5^{I}/_{I_o}} \tag{7}$$

Received: 02/08/2025; Revised: 10/08/2025; Accepted: 15/08/2025; Published: 15/09/2025

The HVL is derived from the graph as

$$HVL(E)_{Expt} = Thickness_{\left(\frac{Final\ Gamma\ spectrum\ Intensity\ after\ counting\ time\ (I)}{Initial\ Gamma\ spectrum\ Intensity\ (I_0)}=1/2\right)} \quad (8)$$

3.0 Results and Discussion

3.1 Results

The results include the theoretical estimation of our shielding parameters from established methods and results obtained from experiments and comparisons with theoretical results and results from previous studies. These are discussed further with the aid of tables and graph plots. Tables 1 to 4 shows the elemental compositions of the four shielding materials. Table 5-8 shows the theoretically obtained LAC values for this study. The Source energy was 661 keV and the gamma source is Cs-137. The calculated linear attenuation coefficients (LAC), half value layers (HVL), tenth value layers (TVL), mean free paths (MFP), and lead equivalence values were summarized in Table 5. The plots in figures 3, 4, 5, 6 shows the attenuation curves for different measured thicknesses (in cm) for glass, sawdust composite, clay and acrylic materials, and the interpolation of the 50% attenuation value of thickness (cm) for each material. Table 9 shows the theoretical shielding parameter values. The comparison of the theoretical half value layer ($HVL_{Theor.}$) with the experimental half value layer ($HVL_{Expt.}$) has been summarized in table 10. While the optimal shielding thickness requirements for all the for shielding material sample in this study are itemized in Table 11

3.2 Discussion

3.2.1 Elemental Weight Fractions and Linear Attenuation Coefficient Determination

Carbon, hydrogen, calcium and phosphorous were found to be dominant elements. Glass and acrylic showed high carbon content, while clay and sawdust composite were richer in calcium and phosphorous. The data obtained from the ICPOES and CHNO analyses summarized the overall elemental composition of each selected material according to level of abundance (in fractional weight). Table 4 gives the date for the extracted weight fraction of elemental composition in a sawdust composite material, Carbon showed significant abundance with about 66 % of the weight of the sample followed by Phosphorous (9 %), Calcium (8 %) and Sulphur (4 %). In the case of the glass sample material, as shown in table 2, Carbon showed significant abundance with about 89 % of the weight of the sample followed by Calcium (5 %) and Hydrogen (3 %). Arsenic and mercury were well below detectable limits. For the case of acrylic sample material as depicted in Table 3, about 52 % weight fraction was assigned on Carbon, Hydrogen followed with about 31 % and Nitrogen with about 5 % weight fraction. Lastly, in the case of the clay sample material data in Table 4, Carbon had the highest level of abundance (about 72%) followed by Calcium (10%), then Phosphorus (8 %). A graph plot of figure 1 showed the different sample shielding materials. In terms of material glass has the highest carbon content while acrylic has the highest hydrogen content. Clay and Sawdust have the most significant Calcium and Carbon. For a detailed comparison among sample shielding materials, a combined bar chart -histogram plot in figure 1 describes the weight fractions accordingly.

Table 1: Weight fractions from the ICP-OES and CHNO analyses of the sawdust composite sample

Constituent Element	Density (g/cm³)	weight (%)
C	2.2660	66.7600
H	0.0001	2.1263
N	0.0013	3.0407
O	0.0014	2.8631
S	2.0000	4.0024
Ca	1.5500	8.1323
Mg	1.7380	0.7215
K	0.8560	2.9271
P	1.8230	9.4210
Na	0.9710	-
Mn	1.7380	0.0014
Fe	7.8740	0.0022
Zn	7.1400	0.0013
Cu	8.9600	0.0003
Pb	11.3400	-
Cr	7.1900	-
Ni	8.9070	-
Co	8.9000	-
Se	4.8100	0.0005

Constituent Element	Density (g/cm³)	weight (%)
As	5.7780	-
Hg	13.5460	-
V	6.1100	-
Li	0.5340	-
Ba	3.5100	-
Be	1.8480	-
Sb	6.6900	-
Sn	7.3000	-

Table 2: Weight Fractions from the ICP-OES and CHNO Analyses of the Glass Sample

Constituent Element	Density (g/cm³)	Weight (%)
C	2.2660	89.3663
H	0.0001	3.1809
N	0.0013	0.0083
O	0.0014	0.4410
S	2.0000	0.2866
Ca	1.5500	5.2816
Mg	1.7380	0.1306
K	0.8560	0.9422
P	1.8230	0.3583
Na	0.9710	0.0003
Mn	1.7380	0.0020
Fe	7.8740	0.0008
Zn	7.1400	0.0006
Cu	8.9600	0.0003
Pb	11.3400	-
Cr	7.1900	-
Ni	8.9070	-
Co	8.9000	-
Se	4.8100	-
As	5.7780	-
Hg	13.5460	-
V	6.1100	-
Li	0.5340	-
Ba	3.5100	-
Be	1.8480	-
Sb	6.6900	-
Sn	7.3000	-

Table 3: Weight Fractions from the ICP-OES and CHNO analyses of the acrylic sample

Constituent Element	Density (g/cm³)	Weight (%)
C	2.2660	52.6619
H	0.0001	31.6350
N	0.0013	5.3041
O	0.0014	0.0086
S	0.0030	0.0040
Ca	0.0435	0.0008
Mg	1.7380	0.0072
K	0.8560	0.0003
P	1.8230	0.0900
Na	0.9710	-
Mn	1.7380	-
Fe	7.8740	0.0022
Zn	7.1400	0.0013
Cu	8.9600	0.0003
Pb	11.3400	-

Received: 02/08/2025; Revised: 10/08/2025; Accepted: 15/08/2025; Published: 15/09/2025

Constituent Element	Density (g/cm³)	Weight (%)
Cr	7.1900	-
Ni	8.9070	-
Co	8.9000	-
Se	4.8100	0.0005
As	5.7780	-
Hg	13.5460	-
V	6.1100	-
Li	0.5340	-
Ba	3.5100	-
Be	1.8480	-
Sb	6.6900	-
Sn	7.3000	-

Table 4: Weight Fractions from the ICP-OES and CHNO analyses of the clay sample

Constituent Element	Density (g/cm³)	Weight (%)
C	2.2660	72.1288
H	0.0001	1.9497
N	0.0013	1.6033
O	0.0014	1.5450
S	2.0000	1.9822
Ca	1.5500	9.6553
Mg	1.7380	0.8251
K	0.8560	2.3520
P	1.8230	7.9537
Na	0.9710	-
Mn	1.7380	0.0013
Fe	7.8740	0.0016
Zn	7.1400	0.0012
Cu	8.9600	0.0003
Pb	11.3400	-
Cr	7.1900	-
Ni	8.9070	-
Co	8.9000	-
Se	4.8100	0.0005
As	5.7780	-
Hg	13.5460	-
V	6.1100	-
Li	0.5340	-
Ba	3.5100	-
Be	1.8480	-
Sb	6.6900	-
Sn	7.3000	-

Received: 02/08/2025; Revised: 10/08/2025; Accepted: 15/08/2025; Published: 15/09/2025

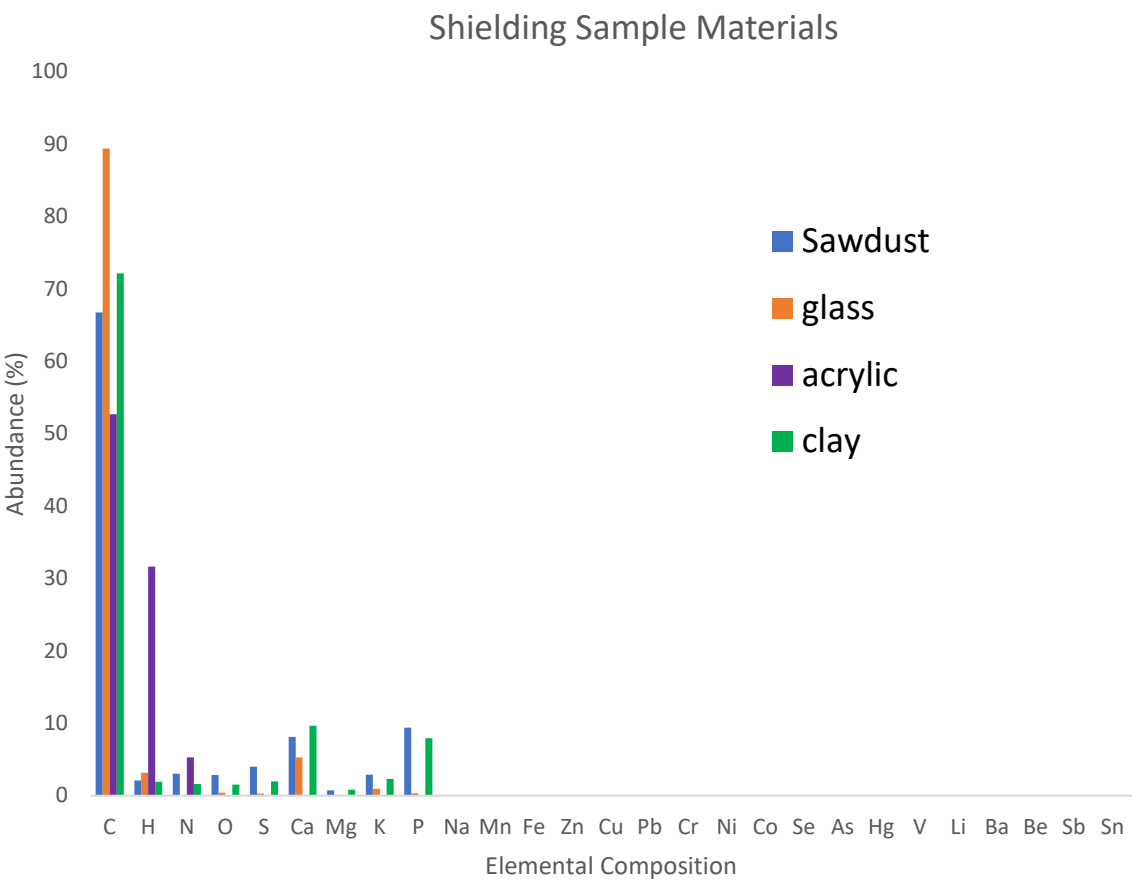

Figure 1: Histogram of weight fractions from the ICP-OES and CHNO Analyses of the sawdust composite, glass, acrylic and clay sample

The data showed that glass in table 6, has the highest LAC with value of about 1.7 cm^{-1}, while the acrylic sample material has the lowest LAC with value of about 0.09 cm^{-1}, clay and sawdust have LAC values of 0.16 cm^{-1} and 0.15 cm^{-1} respectively. This is clearly illustrated in figure 2

Table 5: Weight fractions, energy-dependent mass attenuation coefficients and linear attenuation coefficient of elements based on 661 keV for the sawdust composite sample

Constituent Element	Density (g/cm3)	eight (%)	MAC (cm^2/g)	LAC (cm^{-1})
C	2.2660	66.7600	0.0793	0.1200
H	0.0001	2.1263	0.1378	-
N	0.0013	3.0407	0.0794	-
O	0.0014	2.8631	0.0794	-
S	2.0000	4.0024	0.0793	0.0064
Ca	1.5500	8.1323	0.0796	0.0100
Mg	1.7380	0.7215	0.0784	0.0010
K	0.8560	2.9271	0.0774	0.0019
P	1.8230	9.4210	0.0770	0.0132
Na	0.9710	-	0.0760	-
Mn	1.7380	0.0014	0.0732	-
Fe	7.8740	0.0022	0.0750	-
Zn	7.1400	0.0013	0.0748	-
Cu	8.9600	0.0003	0.0741	-
Pb	11.3400	-	0.1265	-
Cr	7.1900	-	0.0741	-
Ni	8.9070	-	0.0773	-
Co	8.9000	-	0.0740	-
Se	4.8100	0.0005	0.0714	-

Received: 02/08/2025; Revised: 10/08/2025; Accepted: 15/08/2025; Published: 15/09/2025

Constituent Element	Density (g/cm3)	eight (%)	MAC (cm^2/g)	LAC (cm^{-1})
As	5.7780	-	0.0727	-
Hg	13.5460	-	0.1224	-
V	6.1100	-	0.0723	-
Li	0.5340	-	0.0687	-
Ba	3.5100	-	0.0825	-
Be	1.8480	-	0.0705	-
Sb	6.6900	-	0.0796	-
Sn	7.3000	-	0.0791	-
			Estimated LAC (cm^{-1})	0.1526

Table 6: Weight fractions, energy-dependent mass attenuation coefficients and linear attenuation coefficient of elements based on 661 keV (Cs-137 Standard Gamma Source) for the acrylic sample

Constituent Element	Density (g/cm^3)	weight (%)	MAC (cm^2/g)	LAC (cm^{-1})
C	2.2660	52.6619	0.0793	0.0895
H	0.0001	31.6350	0.1378	-
N	0.0013	5.3041	0.0794	-
O	0.0014	0.0086	0.0794	-
S	0.0030	0.0040	0.0793	-
Ca	0.0435	0.0008	0.0796	-
Mg	1.7380	0.0072	0.0784	-
K	0.8560	0.0003	0.0774	-
P	1.8230	0.0900	0.0770	0.0001
Na	0.9710	-	0.0760	-
Mn	1.7380	-	0.0732	-
Fe	7.8740	0.0022	0.0750	-
Zn	7.1400	0.0013	0.0748	-
Cu	8.9600	0.0003	0.0741	-
Pb	11.3400	-	0.1265	-
Cr	7.1900	-	0.0741	-
Ni	8.9070	-	0.0773	-
Co	8.9000	-	0.0740	-
Se	4.8100	0.0005	0.0714	-
As	5.7780	-	0.0727	-
Hg	13.5460	-	0.1224	-
V	6.1100	-	0.0723	-
Li	0.5340	-	0.0687	-
Ba	3.5100	-	0.0825	-
Be	1.8480	-	0.0705	-
Sb	6.6900	-	0.0796	-
Sn	7.3000	-	0.0791	-
			Estimated LAC (cm^{-1})	0.0949

Table 7: Weight fractions, energy-dependent mass attenuation coefficients and linear attenuation coefficient of elements based on 661 keV (Cs-137 Standard Gamma Source) for the glass sample

Constituent Element	Density (g/cm^3)	Weight (%)	MAC (cm^2/g)	LAC (cm^{-1})
C	2.2660	89.3663	0.0793	0.1607
H	0.0001	3.1809	0.1378	-
N	0.0013	0.0083	0.0794	-
O	0.0014	0.4410	0.0794	-
S	2.0000	0.2866	0.0793	0.0005
Ca	1.5500	5.2816	0.0796	0.0065
Mg	1.7380	0.1306	0.0784	0.0002
K	0.8560	0.9422	0.0774	0.0006
P	1.8230	0.3583	0.0770	0.0005
Na	0.9710	0.0003	0.0760	-

Received: 02/08/2025; Revised: 10/08/2025; Accepted: 15/08/2025; Published: 15/09/2025

Constituent Element	Density (g/cm³)	Weight (%)	MAC (cm²/g)	LAC (cm⁻¹)
Mn	1.7380	0.0020	0.0732	-
Fe	7.8740	0.0008	0.0750	-
Zn	7.1400	0.0006	0.0748	-
Cu	8.9600	0.0003	0.0741	-
Pb	11.3400	-	0.1265	-
Cr	7.1900	-	0.0741	-
Ni	8.9070	-	0.0773	-
Co	8.9000	-	0.0740	-
Se	4.8100	-	0.0714	-
As	5.7780	-	0.0727	-
Hg	13.5460	-	0.1224	-
V	6.1100	-	0.0723	-
Li	0.5340	-	0.0687	-
Ba	3.5100	-	0.0825	-
Be	1.8480	-	0.0705	-
Sb	6.6900	-	0.0796	-
Sn	7.3000	-	0.0791	-
			Estimated LAC (cm⁻¹)	0.1690

Table 8: Weight fractions, energy-dependent mass attenuation coefficients and linear attenuation coefficient of elements based on 661 keV (Cs-137 Standard Gamma Source) for the clay sample

Constituent Element	Density (g/cm³)	Weight (%)	MAC (cm²/g)	LAC (cm⁻¹)
C	2.2660	72.1288	0.0793	0.1297
H	0.0001	1.9497	0.1378	-
N	0.0013	1.6033	0.0794	-
O	0.0014	1.5450	0.0794	-
S	2.0000	1.9822	0.0793	0.0031
Ca	1.5500	9.6553	0.0796	0.0119
Mg	1.7380	0.8251	0.0784	0.0011
K	0.8560	2.3520	0.0774	0.0016
P	1.8230	7.9537	0.0770	0.0112
Na	0.9710	0.0000	0.0760	-
Mn	1.7380	0.0013	0.0732	-
Fe	7.8740	0.0016	0.0750	-
Zn	7.1400	0.0012	0.0748	-
Cu	8.9600	0.0003	0.0741	-
Pb	11.3400	-	0.1265	-
Cr	7.1900	-	0.0741	-
Ni	8.9070	-	0.0773	-
Co	8.9000	-	0.0740	-
Se	4.8100	0.0005	0.0714	-
As	5.7780	-	0.0727	-
Hg	13.5460	-	0.1224	-
V	6.1100	-	0.0723	-
Li	0.5340	-	0.0687	-
Ba	3.5100	-	0.0825	-
Be	1.8480	-	0.0705	-
Sb	6.6900	-	0.0796	-
Sn	7.3000	-	0.0791	-
			Estimated LAC (cm⁻¹)	0.1586

Received: 02/08/2025; Revised: 10/08/2025; Accepted: 15/08/2025; Published: 15/09/2025

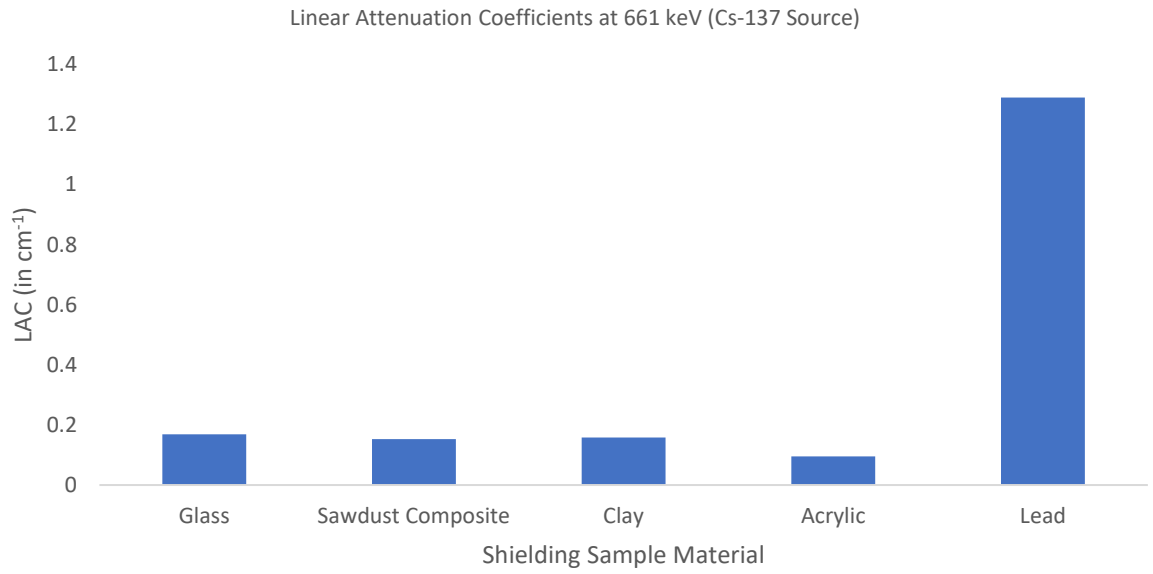

Figure 2: Bar graph of Linear Attenuation Coefficients at 661 keV (Cs-137 Source) for the sawdust composite, glass, acrylic and clay sample

3.2.2 Attenuation Coefficients and Shielding Parameters Calculation

From the calculated linear attenuation coefficients (LAC), half value layers (HVL), tenth value layers (TVL), mean free paths (MFP), and lead equivalence values as summarized in Table 5, Glass was found to have the highest LAC (0.169 cm^{-1}) and the lowest HVL and TVL, indicating the most effective gamma attenuation among the tested materials.

Table 9: Summary of Shielding Parameters at 661 keV

Source: Cs-137 ($T_{1/2}$=30 y, E= 661 keV)

Attenuation		Glass	Sawdust Composite	Clay	Acrylic	Lead
	LAC (cm^{-1})	0.1690	0.1526	0.1586	0.0949	1.2903[a]
~50%	HVL (cm)	4.1006	4.5413	4.3695	7.3075	0.5372
~90%	TVL (cm)	13.6248	15.0890	14.5182	24.2750	1.7846
	MFP (cm)	5.9172	6.5531	6.3052	10.5425	0.7750
~90%	Lead Equivalence (cm Pb)	4.0610	4.0610	4.0610	4.0610	1.7846

Source: Hubbel and Seltzer Mass Attenuation database, NIST, 1995

3.2.3 Experimental Half Value Layer Estimation:

The values of ratio for the Cs-137 spectrum intensity (I) with the attenuation material obstruction, to the Cs-137 spectrum intensity (I_0) without the attenuation material obstruction, (I/I_0) were collected and the plot of attenuation (%) with respect to the sample material thicknesses (cm) were obtained. The interpolated thicknesses corresponding to the 50 percent relative intensity, 50% I/I_0 for glass, sawdust composite, clay and acrylic shielding sample material have been obtained as 3.953, 4.5022, 4.2426, 6.54 respectively.

Received: 02/08/2025; Revised: 10/08/2025; Accepted: 15/08/2025; Published: 15/09/2025

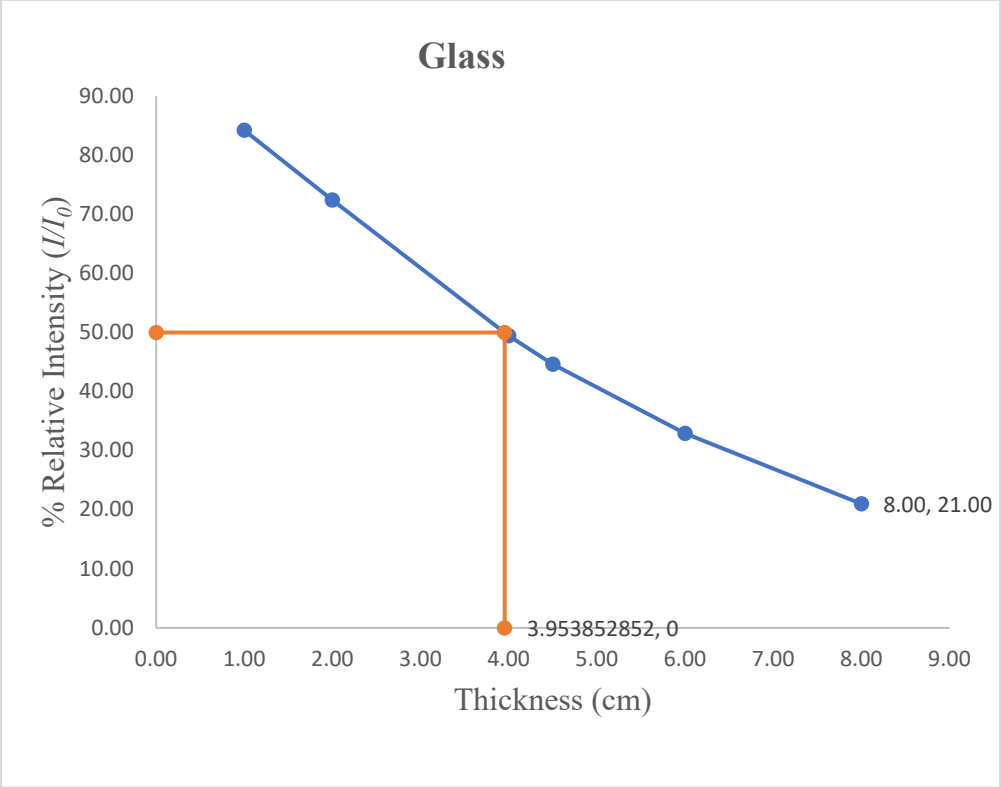

Figure 3: Attenuation Curve for Glass Sample material under Cs-137 for different thickness and the HVL (50 %) interpolated attenuation thickness for the sample

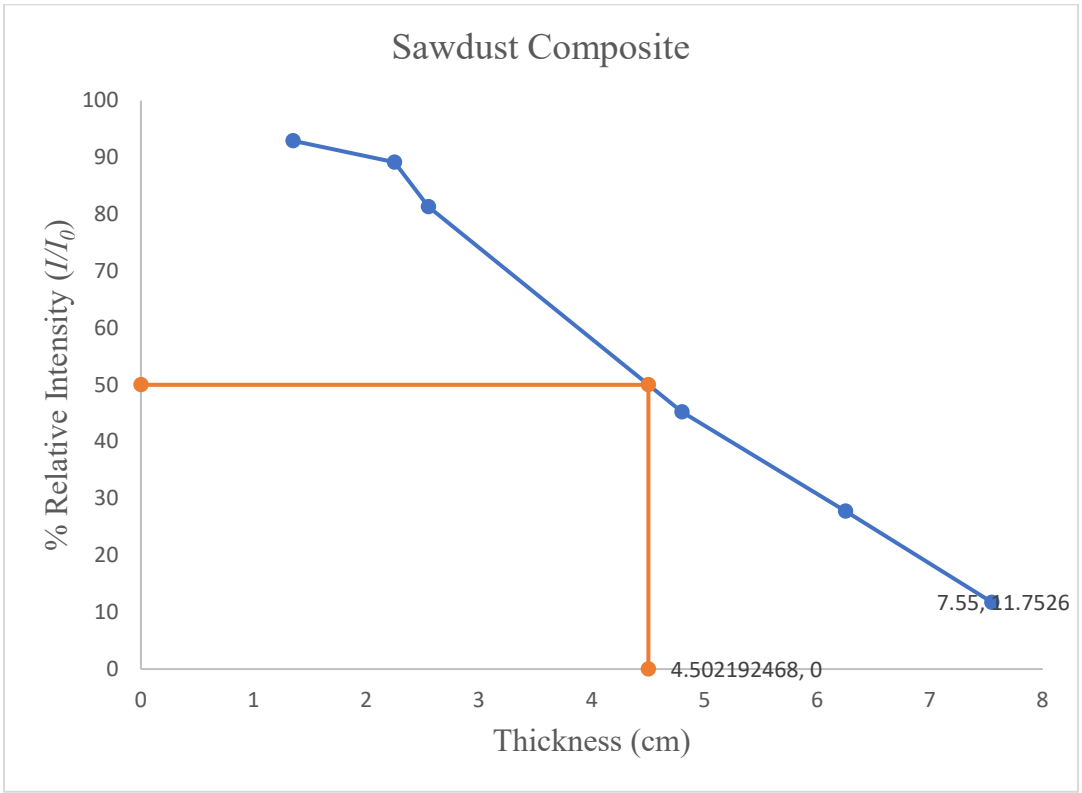

Figure 4: Attenuation Curve for Sawdust Composite Sample material under Cs-137 for different thickness and the HVL (50 %) interpolated attenuation thickness for the sample

Received: 02/08/2025; Revised: 10/08/2025; Accepted: 15/08/2025; Published: 15/09/2025

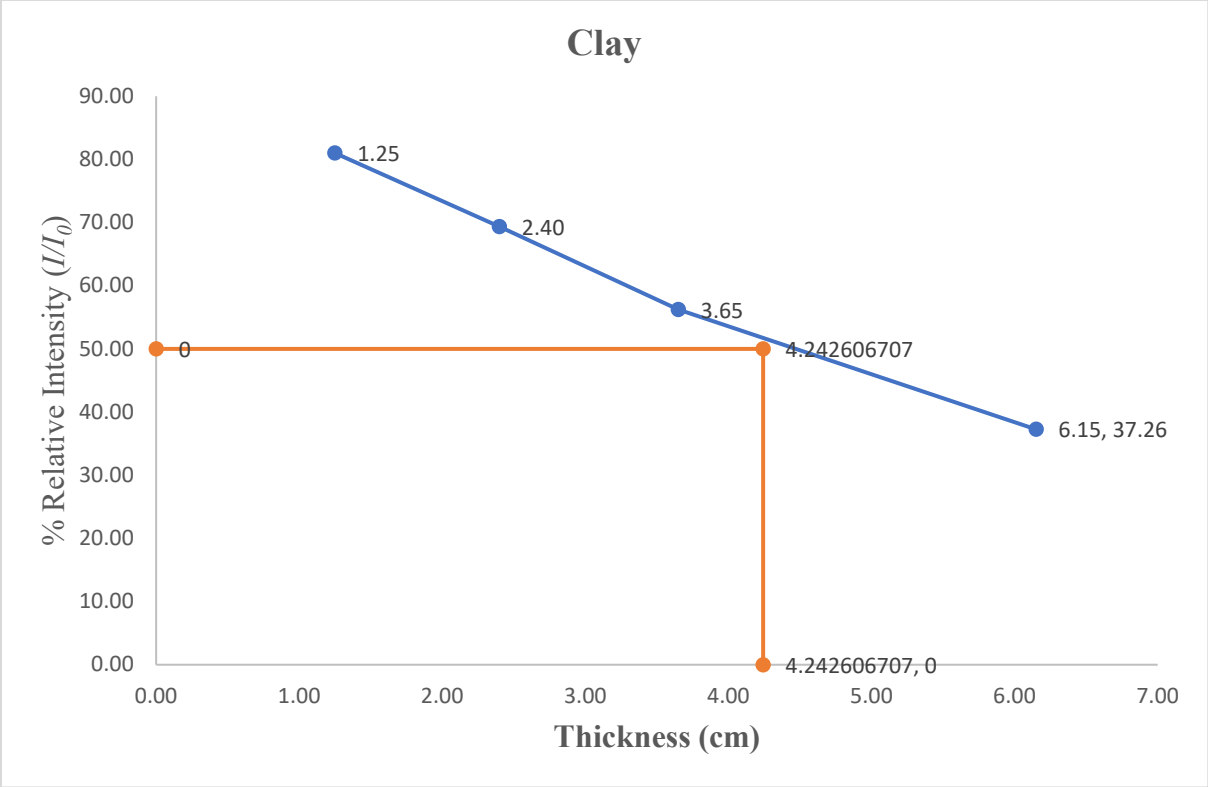

Figure 5: Attenuation Curve for Clay Sample material under Cs-137 for different thickness and the HVL (50 %) interpolated attenuation thickness for the sample

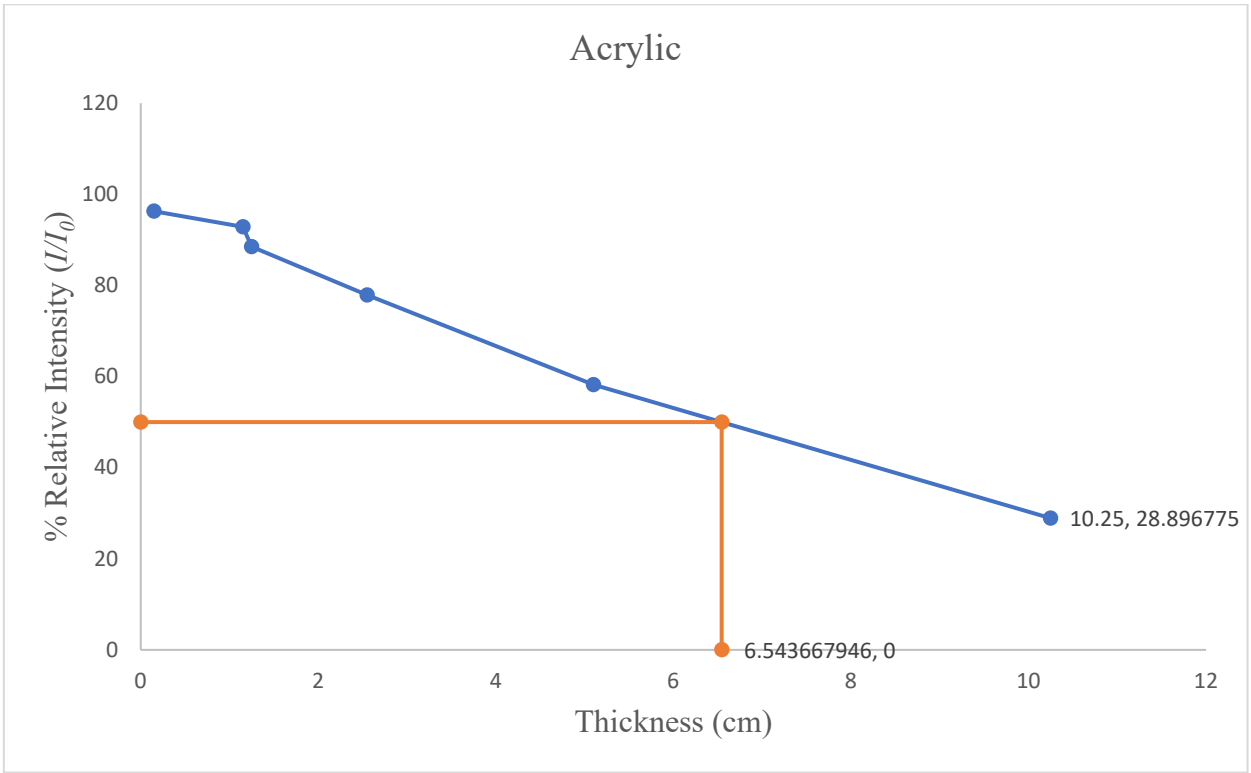

Figure 6: Attenuation Curve for Acrylic Sample material under Cs-137 for different thickness and the HVL (50 %) interpolated attenuation thickness for the sample

3.2.4 Comparison of Theoretical Half Value Layer ($HVL_{Theor.}$) with Experimental Half Value Layer ($HVL_{Expt.}$)

The experimental HVL values obtained for glass, sawdust composite, clay and acrylic were 3.95 cm, 4.50 cm, 4.24 cm and 6.54 cm as opposed to the theoretical values of 4.10 cm, 4.54 cm, 4.37 cm and 7.31 cm respectively. The experimental values differed from theoretical values by 3.73%, 0.87%, 2.99 % and 11.73% respectively.

Received: 02/08/2025; Revised: 10/08/2025; Accepted: 15/08/2025; Published: 15/09/2025

3.2.5 Required Shielding Thickness

To achieve approximately 99.99% attenuation, the minimum required shielding thicknesses were calculated using the HVL values. The results were summarized in Table 11. Glass requires the least thickness (54.49 cm) while acrylic requires the most (97.10 cm).

3.2.6 Comparison with other related studies

In this study pure glass most especially from borosilicate glass type have been reported to have linear attenuation coefficient and HVL values (0.1941 cm^{-1}, 3.57 cm) [Ghafoor and Shawn,2023] similar to the ones reported (0.1690 cm^{-1}, 4.100 cm) in this study. The reported values of LAC and HVL were higher (4.10 cm) than those reported in some studies (1.5-2.0 cm,.3.20 cm) [Yasmin2018; Saleh,2024] were due to reinforced glass-composite types. In the case of the reported clay sample, the obtained values of LACs in this study (0.1586 cm) compared with minimum deviations from those of reported studies (0.1479 cm^{-1}) (Chikkappa,2013). Similarly, Acrylic sample LAC values reported in this study (0.0949 cm^{-1},) deviated from some reported values (0.08401 cm^{-1}, 0.103 cm^{-1}) [Alabsy,2024] of pure acrylic in previous studies. Lastly, Sawdust generally have not had a great reputation when it comes to gamma shielding, since it is mostly considered for low energy photon and/or neutron shielding applications (Shamsuzzaman,2019) but when reinforced with some melted Styrofoam material, its composite gives comparable LAC to glass and glass. Not much interested have been on sawdust-Styrofoam composite in reported studies.

Table 10: Summary of Comparison of Theoretical HVL to Experimental HVL for the Selected Sample Materials in the presence of a Cs-137 (661 keV) Standard Source

Source: Cs-137 ($T_{1/2}$=30 y)661 keV

Attenuation	**Glass**		**Sawdust Composite**		**Clay**		**Acrylic**	
LAC (cm)	Theoretical	Experimental	theoretical	Experimental	theoretical	Experimental	theoretical	Experimental
	0.1690		0.1526		0.1586		0.0949	
HVL (cm)	4.1006	3.953	4.5413	4.5022	4.3695	4.2426	7.3075	6.54
% difference	3.733877301		0.868464306		2.9910904		11.735474	

Table 11: Required thickness for 99.99% Gamma Attenuation

Material	**HVL (cm)**	**%**	**N**	**x (cm)**
Lead	0.5372	99.99	13.28771	7.138
Glass	4.1006	99.99	13.28771	54.488
Sawdust Comp.	4.5413	99.99	13.28771	60.343
Clay	4.3695	99.99	13.28771	58.061
Acrylic	7.3075	99.99	13.28771	97.100

4.0 Conclusion and Recommendation

This study evaluated the gamma shielding effectiveness of four locally available materials within Ibadan metropolis using elemental analysis, theoretical and experimental calculations. Glass exhibited the highest attenuation coefficient, lowest HVL, TVL, and MFP, making it the most effective material for gamma shielding at 661 keV. In terms of the HVL, this study showed that the glass sample requires a greater thickness (about eight[8x] factors higher to achieve the same level of radiation protection as a solid lead sheet, followed by the Clay sample and Sawdust composite sample (9x) while the acrylic sample required a thickness 14 factors higher than lead. However, due to its density, clay and sawdust composite offer a practical balance between effectiveness and weight, making them suitable for broader applications. Acrylic, while useful, may not be ideal for compact shielding where space is limited. Future studies should incorporate experimental validation of shielding using buildup factors and real-time exposure tests under varying energy levels to complement these theoretical findings. Also, extensive study should be carried out on the sawdust composite which tend to be promising for gamma shielding, most especially its thermal stability.

Received: 02/08/2025; Revised: 10/08/2025; Accepted: 15/08/2025; Published: 15/09/2025

References

[1] J. B. Chen, "Comparative study of thermal properties in oxide-modified borate glasses," *Journal of Solid-State Chemistry*, vol. 291, pp. 121–129, 2021.

[2] U. Rilwan, G. M. Aliyu, S. F. Olukotun, M. M. Idris, A. A. Mundi, S. Bello, I. Umar, A. El-Taher, K. A. Mahmoud, and M. I. Sayyed, "Recycling and characterization of bone incorporated with concrete for gamma-radiation shielding applications," *Nuclear Engineering and Technology*, vol. 56, pp. 2828–2834, 2024.

[3] M. Y. Hanfi, A. Saftah, S. J. Alsufyani, M. S. Alqahtani, and K. A. Mahmoud, "Experimental investigation of fired clay bricks for gamma radiation shielding," *Radiation Physics and Chemistry*, vol. 226, p. 112245, 2025.

[4] S. F. Olukotun, S. T. Gbenu, K. O. Oyedotun, O. Fasakin, M. I. Sayyed, G. O. Akindoyin, H. O. Shittu, M. K. Fasasi, M. U. Khandaker, H. Osman, and B. H. Elesawy, "Fabrication and characterization of clay-polyethylene composite opted for shielding of ionizing radiation," *Crystals*, vol. 11, no. 1068, 2021.

[5] A. H. Sevinç and M. Y. Durgun, "A novel epoxy-based composite with eggshell, PVC sawdust, wood sawdust and vermiculite: An investigation on radiation absorption and various engineering properties," *Construction and Building Materials*, vol. 300, p. 123985, 2021.

[6] I. C. Okereke, B. Adebo, E. Oyekunle, E. O. Agbenyi, L. Enin, and K. Adam, "Assessing shielding adequacy of selected radiological facilities to ascertain radiation safety in Ibadan metropolis," *Environmental Contaminants Reviews (ECR)*, vol. 7, no. 1, pp. 6–17, 2024.

[7] P. Rawat, M. K. Singh, and D. S. Chauhan, "The use of glass in architecture: A sustainable approach," *Materials Today: Proceedings*, vol. 8, pp. 513–520, 2019.

[8] L. X. Zhao and H. Y. Wang, "The influence of bismuth oxide on the thermal conductivity and expansion of borate glasses," *Glass Science and Technology*, vol. 76, pp. 235–242, 2013.

[9] E. K. Ahmed, H. M. Mahran, M. F. Alrashdi, and M. Elsafi, "Studying the shielding ability of different cement mortars against gamma-ray sources using waste iron and BaO microparticles," *Nexus of Future Materials*, vol. 1, pp. 1–5, 2024.

[10] E. Toto, L. Lambertini, S. Laurenzi, and M. G. Santonicola, "Recent advances and challenges in polymer-based materials for space radiation shielding," *Polymers*, vol. 16, p. 382, 2024.

[11] N. J. Abualroos, M. I. Idris, H. Ibrahim, M. I. Kamaruzaman, and R. Zainon, "Physical, mechanical, and microstructural characterisation of tungsten carbide-based polymeric composites for radiation shielding application," *Scientific Reports*, vol. 14, p. 1375, 2024.

[12] G. Álvarez-Cortez, et al., "Design and study of novel composites based on EPDM rubber containing bismuth (III) oxide and graphene nanoplatelets for gamma radiation shielding," *Polymers*, vol. 16, p. 633, 2024.

[13] N. Hesham, H. M. Abu-Zeid, A. Nada, I. S. Yahia, M. S. A. Hussien, H. M. Diab, M. A. Ali, A. T. Mosleh, and D. Elfiky, "Development of PMMA composites with tungsten trioxide for improved gamma radiation shielding in microsatellites," *Radiation Physics and Chemistry*, vol. 226, p. 112245, 2025.

[14] M. M. Dorostkar and A. A. Saray, "Development of PMMA based polymer composite incorporating WO3 for gamma radiation shielding using synthesis and Monte Carlo simulation," *Radiation Physics and Chemistry*, vol. 226, p. 112246, 2025.

[15] N. A. Muhammad, B. Armynah, and D. Tahir, "High transparent wood composite for effective X-ray shielding applications," *Materials Research Bulletin*, vol. 154, p. 111930, 2022.

[16] M. Shamsuzzaman, M. A. M. Khan, M. M. H. Bhuiyan, M. S. Rahman, M. J. H. Khan, D. Paul, and D. R. Sarkar, "Attenuation property of wood and fiber reinforced polymer composite materials for neutron and gamma radiation shielding," *American Journal of Materials Science*, vol. 9, no. 1, pp. 8–14, 2019.

[17] K. Ninyong, E. Wimolmala, N. Sombatsompop, and K. Saenboonruang, "Properties of natural rubber (NR) and wood/NR composites as gamma shielding materials," *IOP Conf. Ser.: Mater. Sci. Eng.*, vol. 526, p. 012038, 2019.

[18] F. Bouzarjomehri, T. Baya, M. H. Dashti, J. Ghisari, and N. Abdoli, "60Co γ-ray attenuation coefficient of barite concrete," *Iran J. Radiat. Res.*, vol. 2, no. 4, pp. 71–75, 2006.

[19] National Council on Radiation Protection and Measurement, *Permissible Dose from External Sources of Ionizing Radiation*, Washington, D. C.: NCRP, 1954.

[20] A. H. A. Hamoud, A. R. Khan, and J. M. Pathan, "Investigation of radiation shielding properties for some soil samples for use in shields against gamma-rays from different nuclides," *Bull. Pure Appl. Sci.*, vol. 38, no. 1, pp. 32–45, 2019.

[21] D. A. Aloraini, A. H. Almuqrin, K. M. Kaky, M. I. Sayyed, and M. Elsafi, "Radiation shielding capability and exposure buildup factor of cerium (IV) oxide-reinforced polyester resins," *e-Polymers*, vol. 23, p. 20230128, 2023.

Received: 02/08/2025; Revised: 10/08/2025; Accepted: 15/08/2025; Published: 15/09/2025

[22] J. H. Hubbell and S. M. Seltzer, *Tables of X-ray Mass Attenuation Coefficients and Mass Energy-Absorption Coefficients 1 keV to 20 MeV for Elements Z = 1 to 92 and 48 Additional Substances of Dosimetric Interest*, NISTIR-5632, Gaithersburg: NIST, 1995.

[23] H. O. Tekin, G. ALMisned, S. A. M. Issa, and H. M. H. Zakaly, "A rapid and direct method for half value layer calculations for nuclear safety studies using MCNPX Monte Carlo code," *Nuclear Engineering and Technology*, vol. 54, pp. 1–10, 2022.

[24] A. B. Azeez, S. M. Kahtan, M. A. A. Mohd, H. Kamaradin, V. S. Andrie, and A. R. Rafiz, "The effect of various waste materials contents on the attenuation level of anti-radiation shielding concrete," *Materials*, vol. 27, pp. 1–7, 2013.

[25] Y. Elmahroug, B. Tellili, and C. Souga, "Calculation of gamma and neutron shielding parameters for some materials polyethylene-based," *Int. J. Phys. Res.*, vol. 3, pp. 33–40, 2013.

[26] I. Michalak, K. Marycz, K. Basińska, and K. Chojnacka, "Using SEM-EDX and ICP-OES to investigate the elemental composition of green macroalga Vaucheria sessilis," *Scientific World Journal*, vol. 2014, p. 891928, 2014.

[27] T. C. F. Silva, J. L. Gomide, and R. B. Santos, "Evaluation of chemical composition and lignin structural features of simarouba versicolor wood on its pulping performance," *Bioresources*, vol. 7, no. 3, pp. 3910–3920, 2012.

[28] M. T. Alabsy, M. I. Abbas, A. Y. El Khatib, and A. M. El Khatib, "Attenuation properties of poly methyl methacrylate reinforced with micro/nano ZrO2 as gamma ray shields," *Scientific Reports*, vol. 14, p. 1279, 2024.

[29] A. Saleh, M. I. Sayyed, A. Kumar, and F. E. Mansour, "Synthesis and gamma ray shielding efficiency of borosilicate glasses doped with zinc oxide: Comparative study," *Silicon*, vol. 16, pp. 4427–4435, 2024.

[30] M. Shamsuzzaman, M. A. M. Khan, M. M. H. Bhuiyan, M. S. Rahman, M. J. H. Khan, D. Paul, and D. R. Sarkar, "Attenuation property of wood and fiber reinforced polymer composite materials for neutron and gamma radiation shielding," *American Journal of Materials Science*, vol. 9, no. 1, pp. 8–14, 2019

Received: 02/08/2025; Revised: 10/08/2025; Accepted: 15/08/2025; Published: 15/09/2025